Formation of a junction between TiO_2 and β-Bi_2O_3 to enable efficient visible-light harvesting in advanced oxidation processes for waste water treatment

Gregor Žerjav

Department of Inorganic Chemistry and Technology,
National Institute of Chemistry, Ljubljana, Slovenia
gregor.zerjav@ki.si

NOWELTIES – 3rd Project Meeting & ATC2, 16th-18th September 2020, Zagreb, Croatia

Heterogeneous Photocatalysis

Heterogeneous photocatalysis, utilizing either **ultraviolet (UV)** or **visible light irradiation** of a **catalyst** (semiconductor), is one of the most studied **AOPs** for wastewater treatment.

The **main role of a catalyst** in the photocatalytic reaction is to produce **reactive oxygen species (ROS)**, which lead to the photocatalytic transformation of liquid-dissolved pollutants and ultimately produce H_2O and CO_2 (**mineralization**).

Semiconductor excited with energy (***hu***) equal to or greater than the **band gap energy** generates electrones ($\mathbf{e^-}$) and holes ($\mathbf{h^+}$);

(i) reduce and oxidize substrates adsorbed on catalyst surface and produce **ROS** ($\mathbf{O_2^{-\cdot}}$ **, OH·, etc.**);

(ii) recombine with each other (**heat**).

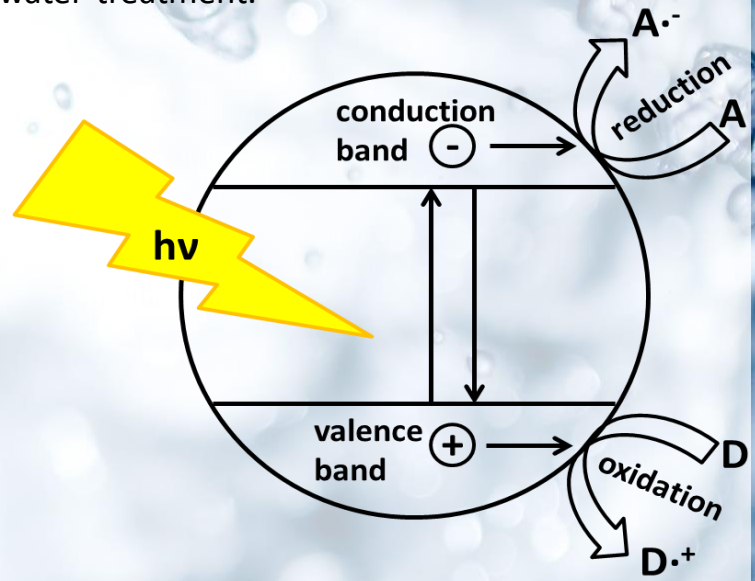

Fig. 1. Photo-induced formation of charge carriers and corresponding reaction pathways in a semiconductor photocatalyst.

TiO_2

Most used catalyst is **TiO_2**:

- **Advantages:** high photocatalytic activity, photo- and chemical stability, low cost, water insolubility under most conditions and non-toxicity;

- **Drawbacks**: (i) wide band gap energy of **3.2-3.4 eV** and (ii) **fast electron-hole recombination**.

Fig. 2. TiO_2 in powdered form.

different approaches to improve the catalytic activity of TiO_2 toward waste water treatment were tested:

combining with **reduced graphene oxide (rGO);**

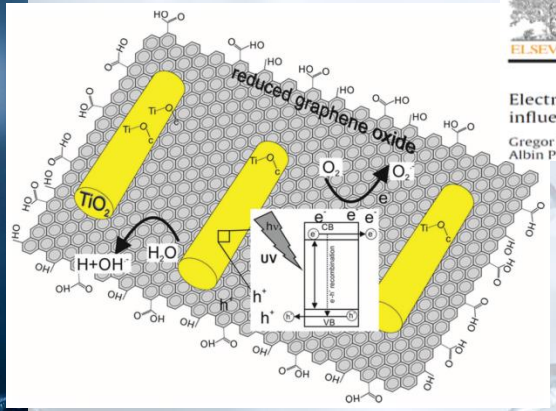

combining with **tungsten oxide (WO_3);**

Applied Catalysis B: Environmental 209 (2017) 273–284
Contents lists available at ScienceDirect
Applied Catalysis B: Environmental
journal homepage: www.elsevier.com/locate/apcatb

Electron trapping energy states of TiO_2–WO_3 composites and their influence on photocatalytic degradation of bisphenol A

Gregor Žerjav[a,*], Muhammad Shahid Arshad[a], Petar Djinović[a], Janez Zavašnik[b], Albin Pintar[a]

Nanoscale
PAPER
View Article Online
View Journal | View Issue
Check for updates
Cite this: Nanoscale, 2017, 9, 4578

Improved electron–hole separation and migration in anatase TiO_2 nanorod/reduced graphene oxide composites and their influence on photocatalytic performance†

Gregor Žerjav,*[a] Muhammad Shahid Arshad,[a] Petar Djinović,[a] Ita Junkar,[b] Janez Kovač,[b] Janez Zavašnik[c] and Albin Pintar[a]

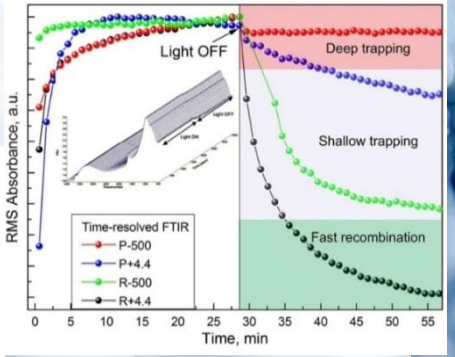

Conclusions:
- decreased electron-hole recombination rate under UVA light illumination
- **determination of the right amount of TiO_2 dopant is crucial to achieve efficient catalyst activity**
- the morphology of TiO_2 can influence the properties of a composite

Aim: Combine TiO_2 with low-band gap semiconductor β-Bi_2O_3 and to use it as visible-light photosenzitizer

Solution combustion synthesis procedures of the catalysts

$Bi(NO_3)_3 * 5H_2O$

+

$C_6H_8O_7 * H_2O$

+

0.04 M HNO_3

↓ stirred for 1 h

PEG-5800

↓ stirred for 1 h

TiO_2 (DT-51) →

↓ stirred for 3 h

calcination 300 °C/4 h

Žerjav et. A., *Catalysis today*, 2020, doi: 10.1016/j.cattod.2020.03.053.

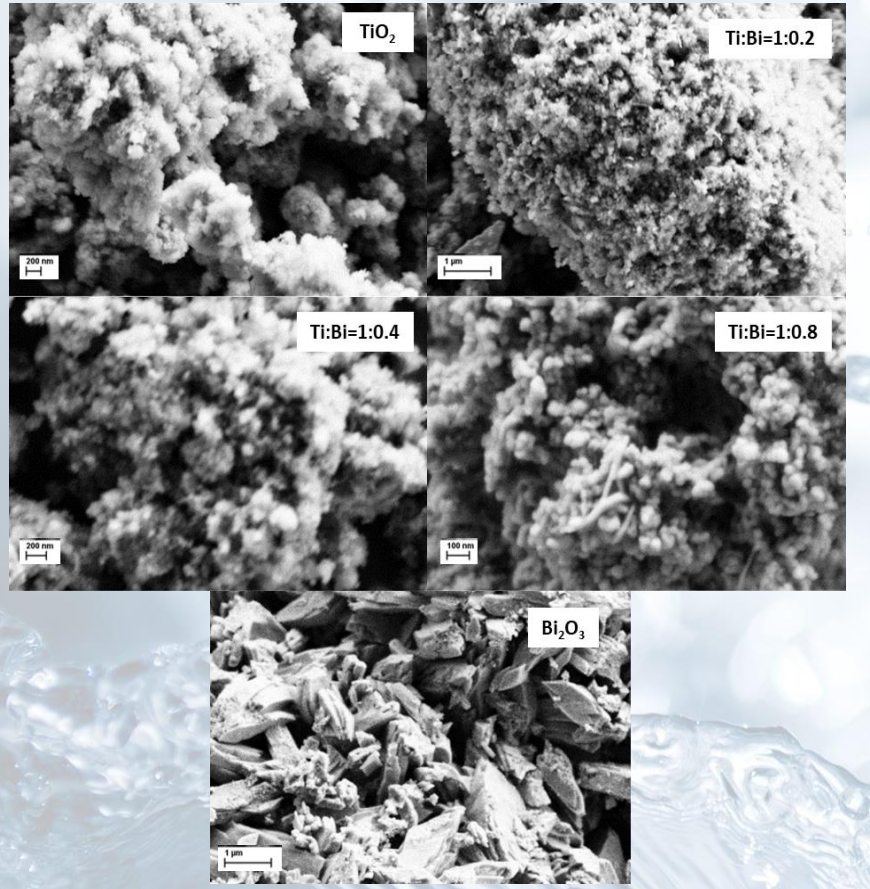

Fig. 1. SEM micrographs of prepared catalysts.

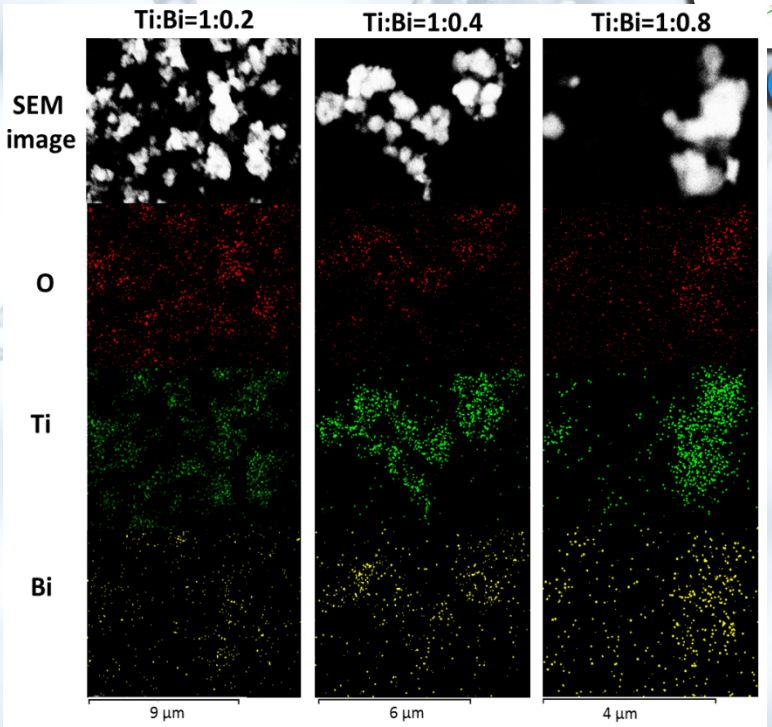

Fig. 2. SEM-EDX elemental mapping conducted on prepared TiO_2-β-Bi_2O_3 composites.

Žerjav et. A., *Catalysis today*, 2020, doi: 10.1016/j.cattod.2020.03.053.

Sample		wt. %			Ti:Bi= actual ratio
		O	Ti	Bi	
TiO_2		54	47	–	–
β-Bi_2O_3		15	–	85	–
Ti:Bi = (nominal ratio)	1:0.2	51	41	8	1:0.20
	1:0.4	45	40	15	1:0.38
	1:0.8	43	33	24	1:0.73

Table 1. Results of SEM-EDX analysis of the prepared catalysts.

Sample		S_{BET} (m^2/g)	V_{pore} (cm^3/g)	d_{pore} (nm)
TiO_2		85.8	0.29	13.7
β-Bi_2O_3		4.7	0.02	16.5
Ti:Bi =	1:0.2	79.0	0.26	13.1
	1:0.4	69.9	0.25	13.4
	1:0.8	60.0	0.20	13.8

Table 2. BET specific surface area (S_{BET}), total pore volume (V_{pore}) and average pore diameter (d_{pore}).

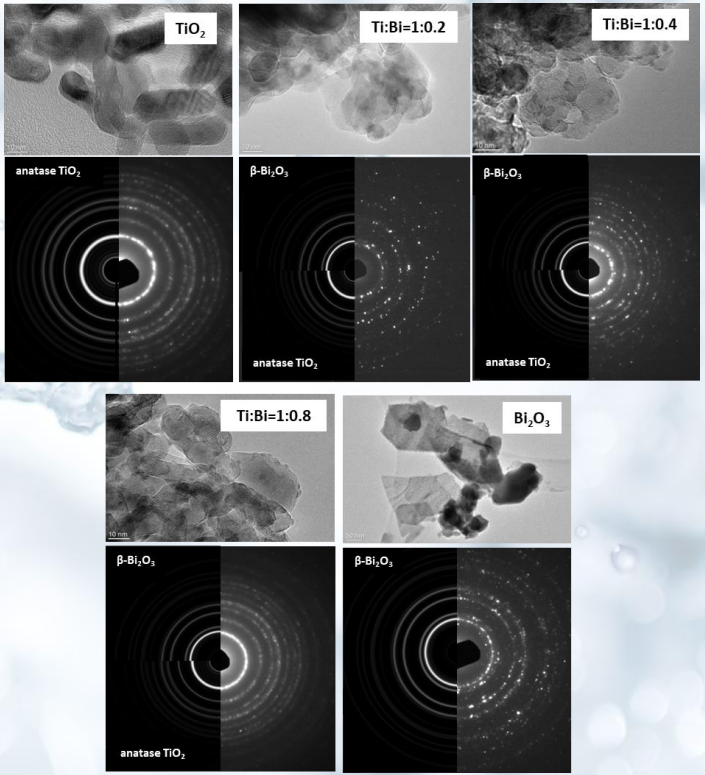

Fig. 3. TEM micrographs of prepared catalysts. Figures below show experimental selected area electron diffraction (SAED) patterns of prepared catalysts compared with simulation patterns of anatase TiO_2 and Bi_2O_3.

Žerjav et. A., *Catalysis today*, 2020, doi: 10.1016/j.cattod.2020.03.053.

XRD measurements

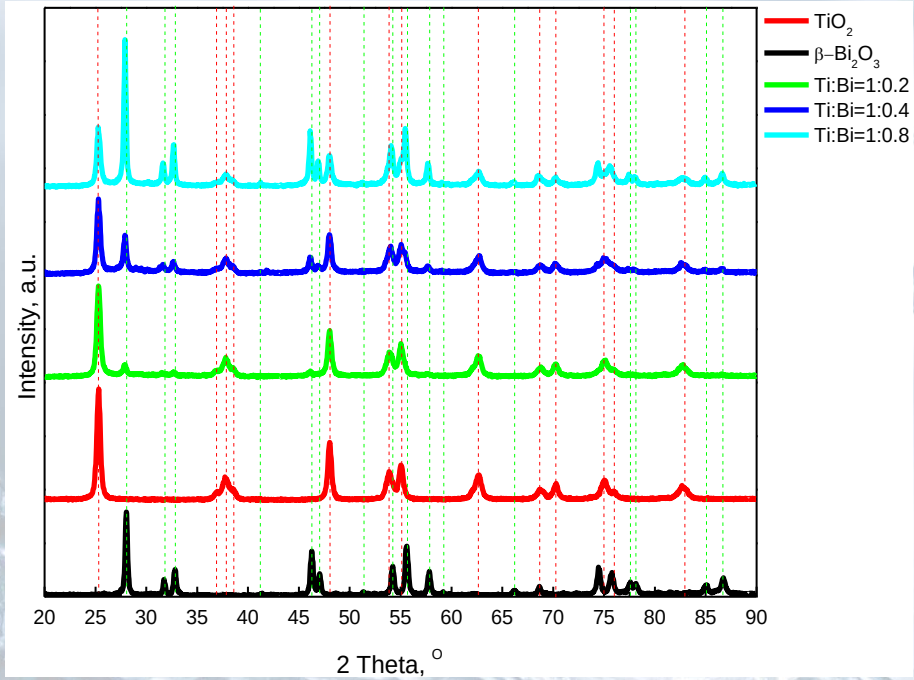

Fig. 4. XRD patterns of the prepared materials (green vertical lines belong to tetragonal (β) Bi_2O_3 (JCPDS 00-027-0050) and red vertical lines to anatase TiO_2 (JCPDS 00-021-1272)).

Sample		Average crystallite size (nm)	
		Anatase TiO_2°	Tetragonal β-Bi_2O_3*
TiO_2		20	–
β-Bi_2O_3		–	31
Ti:Bi=	1:0.2	20	22
	1:0.4	20	25
	1:0.8	20	33

°Average crystallite size of anatase TiO_2 (JCPDS 00-021-1272)
*Average crystallite size of tetragonal β-Bi_2O_3 (JCPDS 00-027-0050)

Table 3. Average anatase TiO_2 and tetragonal β-Bi_2O_3 crystallite size of synthesized catalysts.

Žerjav et. A., *Catalysis today*, 2020, doi: 10.1016/j.cattod.2020.03.053.

UV-Vis DR measurements

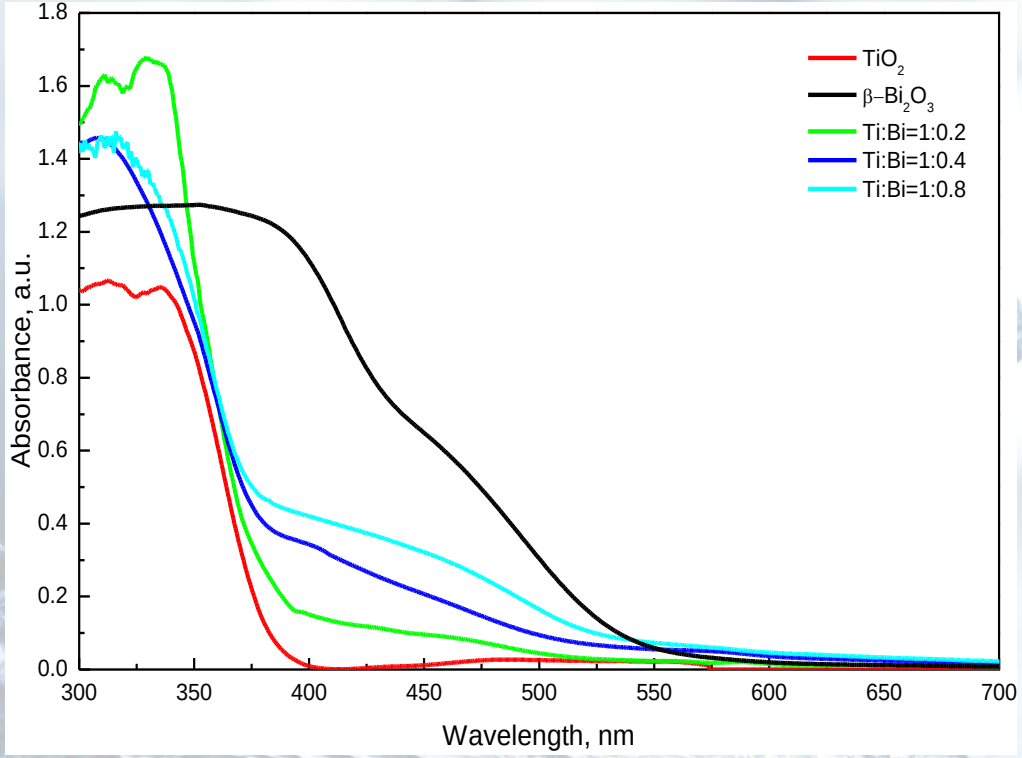

Fig. 5. UV-Vis DR spectra of synthesized catalysts.

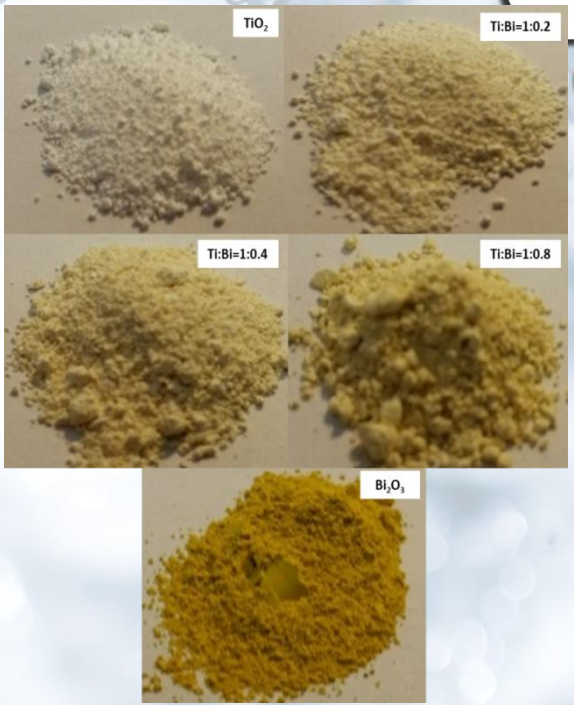

Fig. 6. Photographs of the synthesized catalysts.

Žerjav et. A., *Catalysis today*, 2020, doi: 10.1016/j.cattod.2020.03.053.

EIS measurements

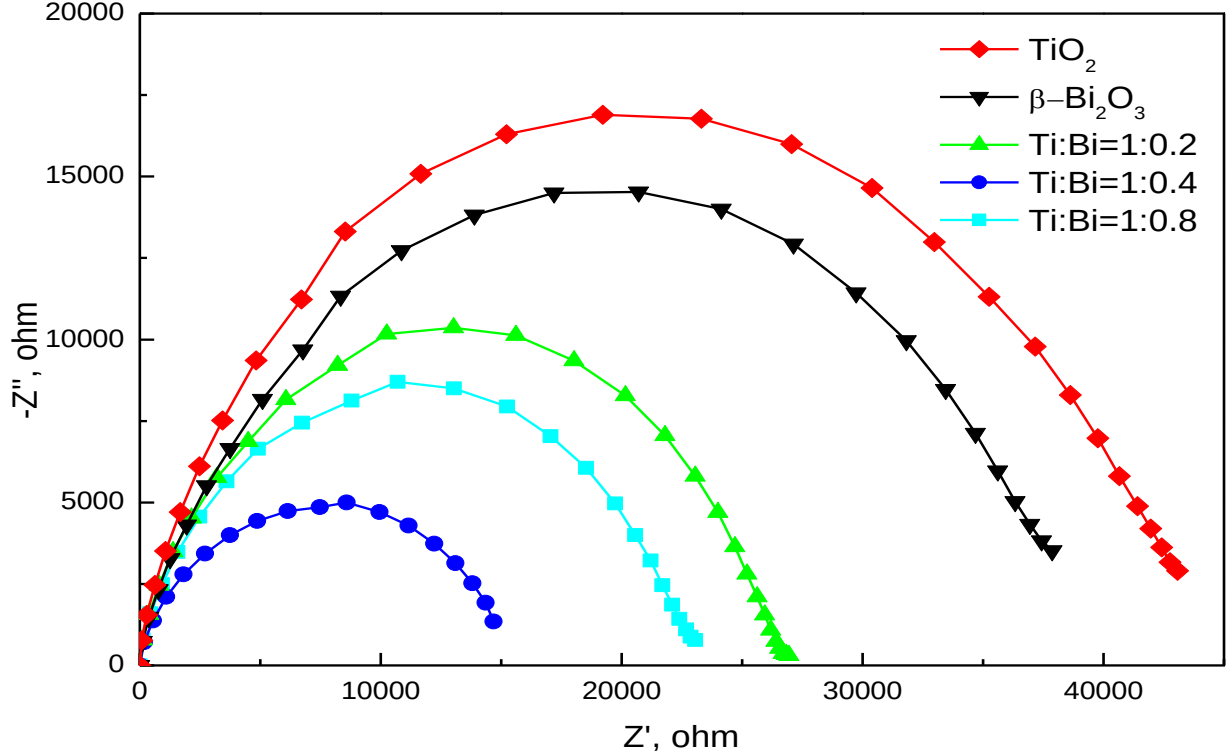

Fig. 7. Electrochemical impedance spectra of prepared catalysts under visible-light illumination.

Žerjav et. A., *Catalysis today*, 2020, doi: 10.1016/j.cattod.2020.03.053.

Photoluminescence (PL) emission spectra of the samples

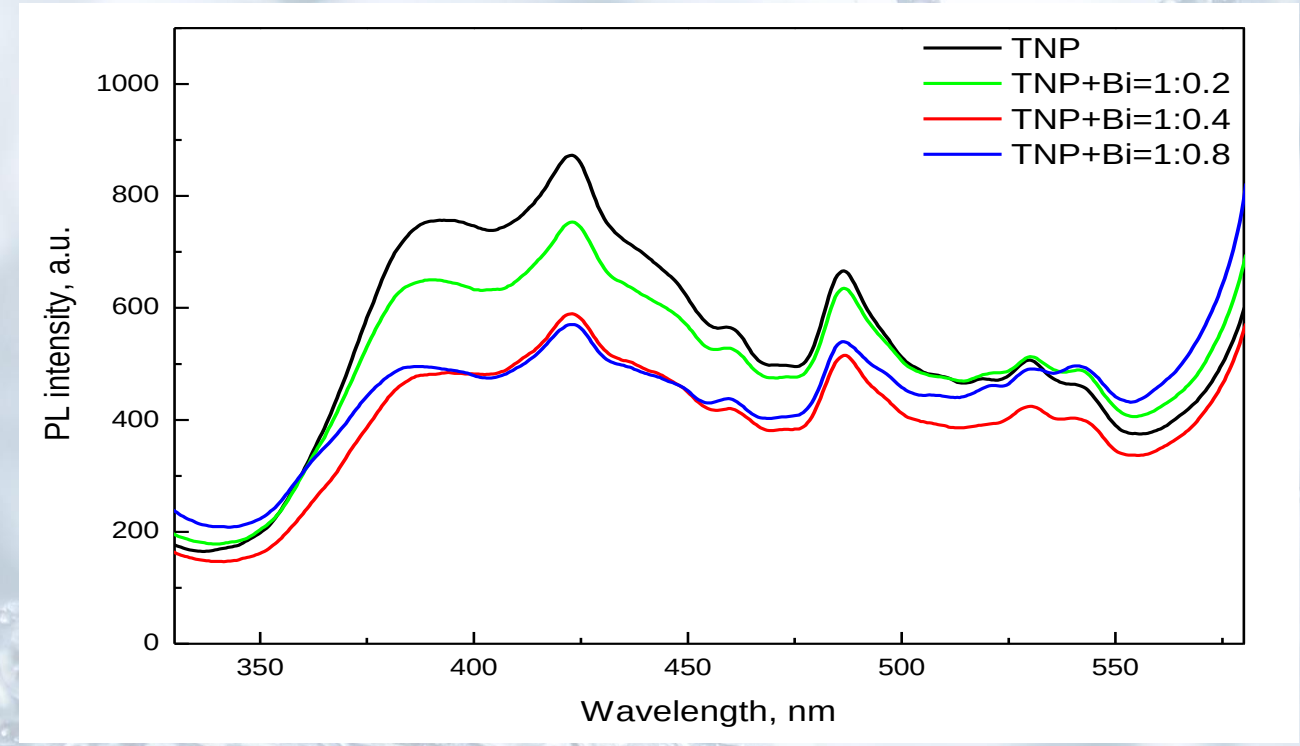

Fig. 8. PL spectra were recorded by means of a UV-Vis fluorescence spectrometer (Perkin Elmer, model LS-55) using λ=300 nm as excitation wavelength at room temperature. The samples were pressed in a holder to get a flat surface before the analysis.

Žerjav et. A., *Catalysis today*, 2020, doi: 10.1016/j.cattod.2020.03.053.

*DMPO in **DMSO → ($O_2^{\cdot-}$)

EPR measurements

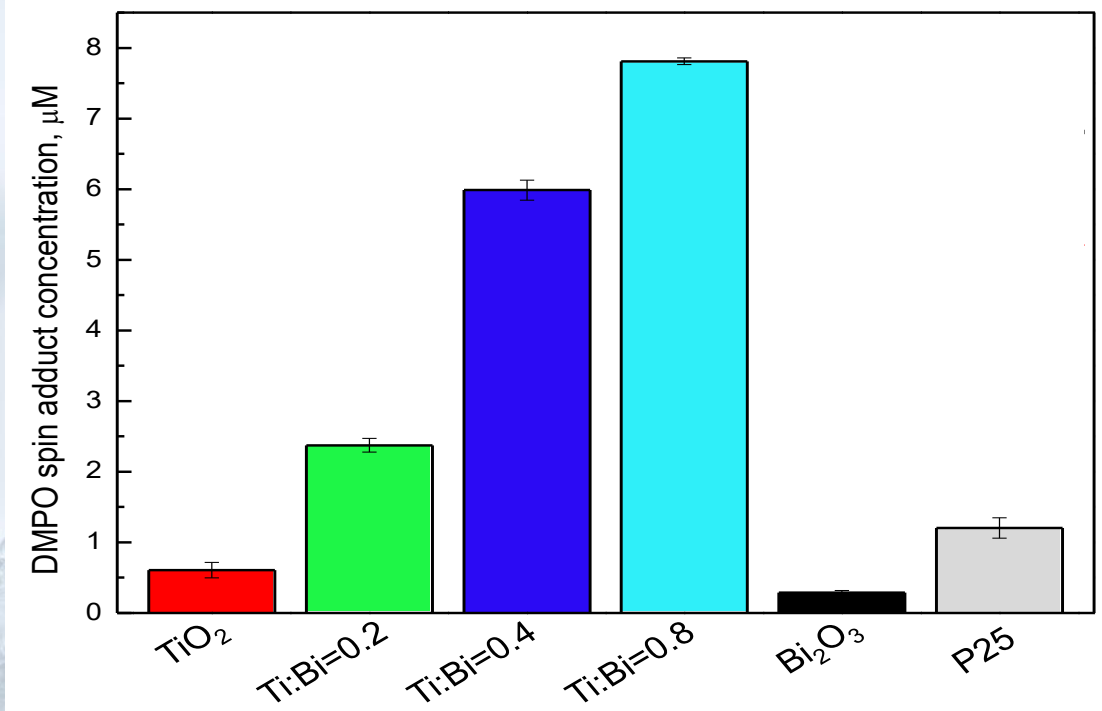

Fig. 9. Concentrations of monitored DMPO spin adducts generated upon 6 min visible-light exposure (160 klx) of DMSO suspensions of studied photocatalysts, both in the presence of DMPO spin trapping agent under air at 295 K.

* 5,5-dimethyl-1-pyrroline N-oxide
** dimethylsulfoxide

$ABTS^{\bullet+} \rightarrow (e^- \text{ and } O_2^{\cdot-})$

visible-light illumination

visible-light illumination

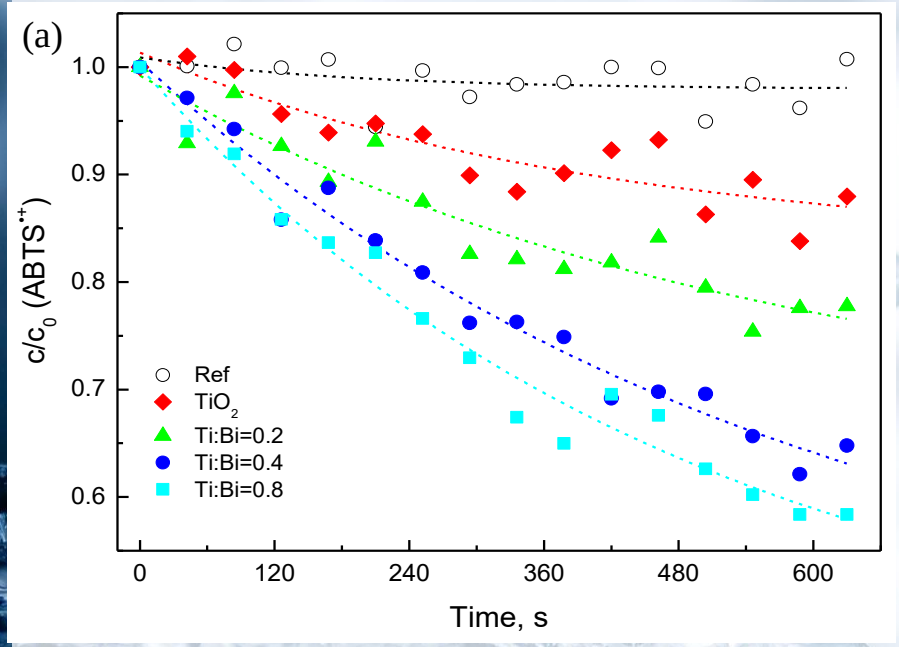

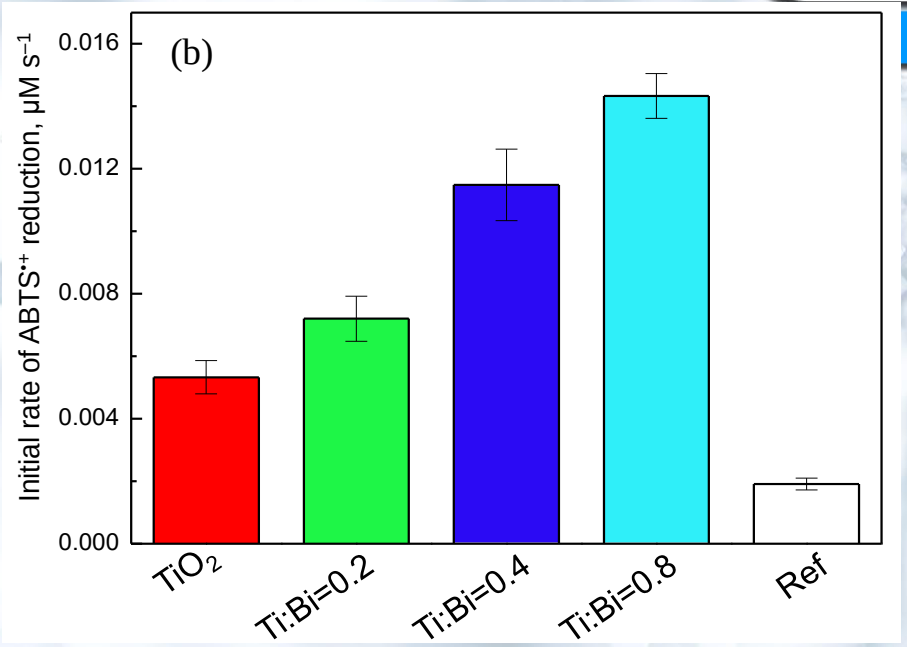

Fig. 10. (a) Dependence of the *cation **ABTS$^{\bullet+}$** relative concentration on the irradiation time measured upon **visible-light exposure** (160 klx) of water suspensions of studied photocatalysts containing $ABTS^{\bullet+}$ under air and photocatalyst-free reference solution. (b) Initial rate of $ABTS^{\bullet+}$ reduction was evaluated from the data presented in (a). Initial concentrations: c_0(catalyst) = 0.8 g/L; $c_0(ABTS^{\bullet+})$ = 12 μM.

* 2,2′-azinobis(3-ethylbenzothiazoline-6-sulfonic acid) diammonium salt

Bisphenol A (BPA) degradation in a slurry batch reactor

Fig. 11. Photocatalytic degradation of BPA (c_0=10 mg/L) in the presence of prepared catalysts irradiated with visible-light (halogen lamp, 150 W, λ_{max} = 520 nm, UV cut off filter at 410 nm) . The catalyst concentration used in the performed experiments was 125 mg/L.

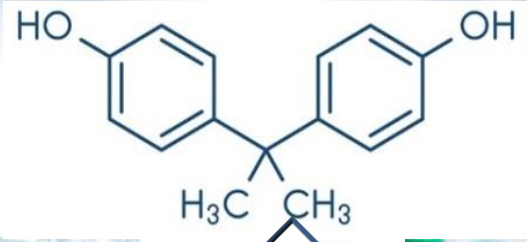

Fig. 12. Bisphenol A (BPA)

Žerjav et. A., *Catalysis today*, 2020, doi: 10.1016/j.cattod.2020.03.053.

Bisphenol A (BPA) degradation in a slurry batch reactor

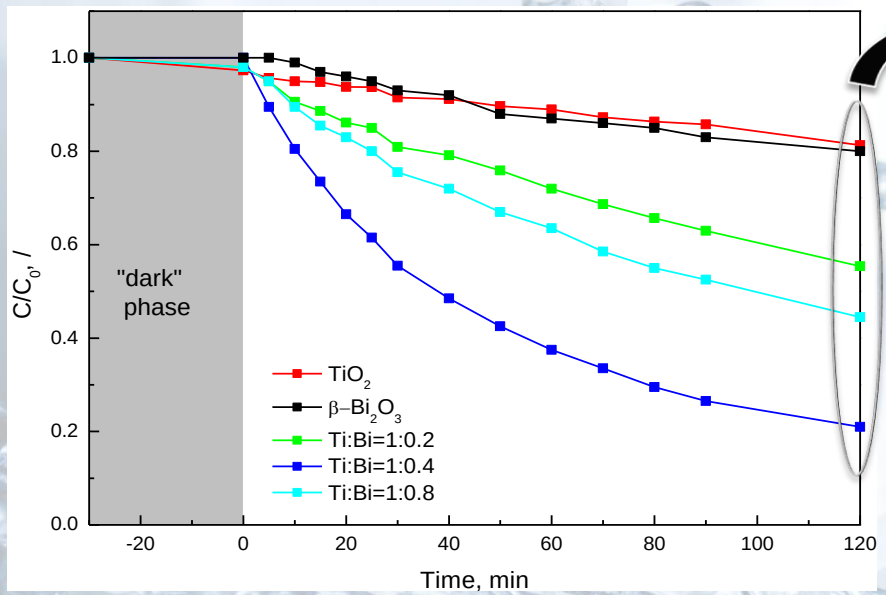

Fig. 13. Photocatalytic degradation of BPA in the presence of prepared catalysts irradiated.

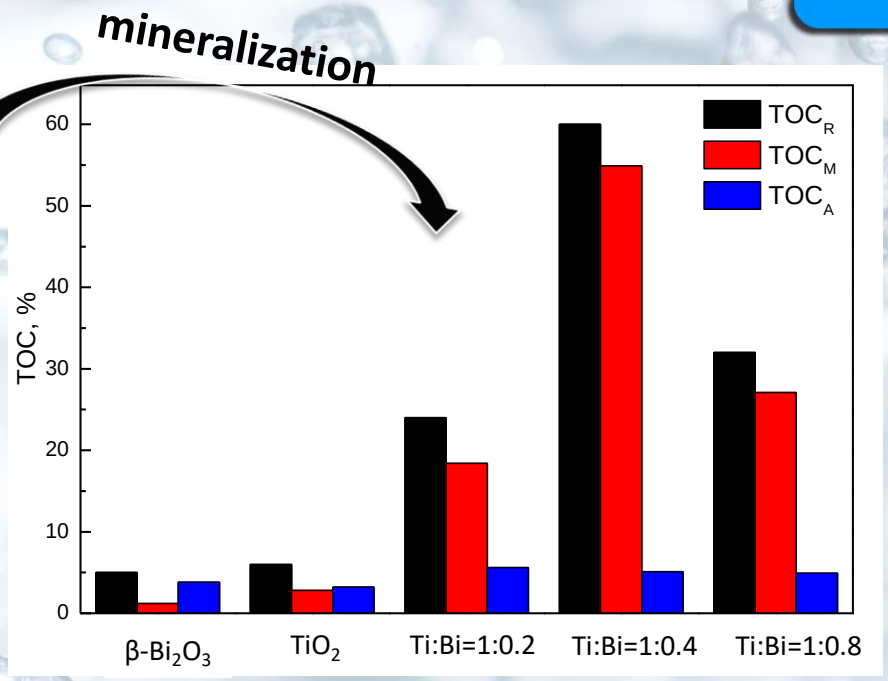

Fig. 14. TOC removal (TOC_R) represents a sum of true TOC conversion (TOC_M) and TOC accumulation (TOC_A).

Žerjav et. A., *Catalysis today*, 2020, doi: 10.1016/j.cattod.2020.03.053.

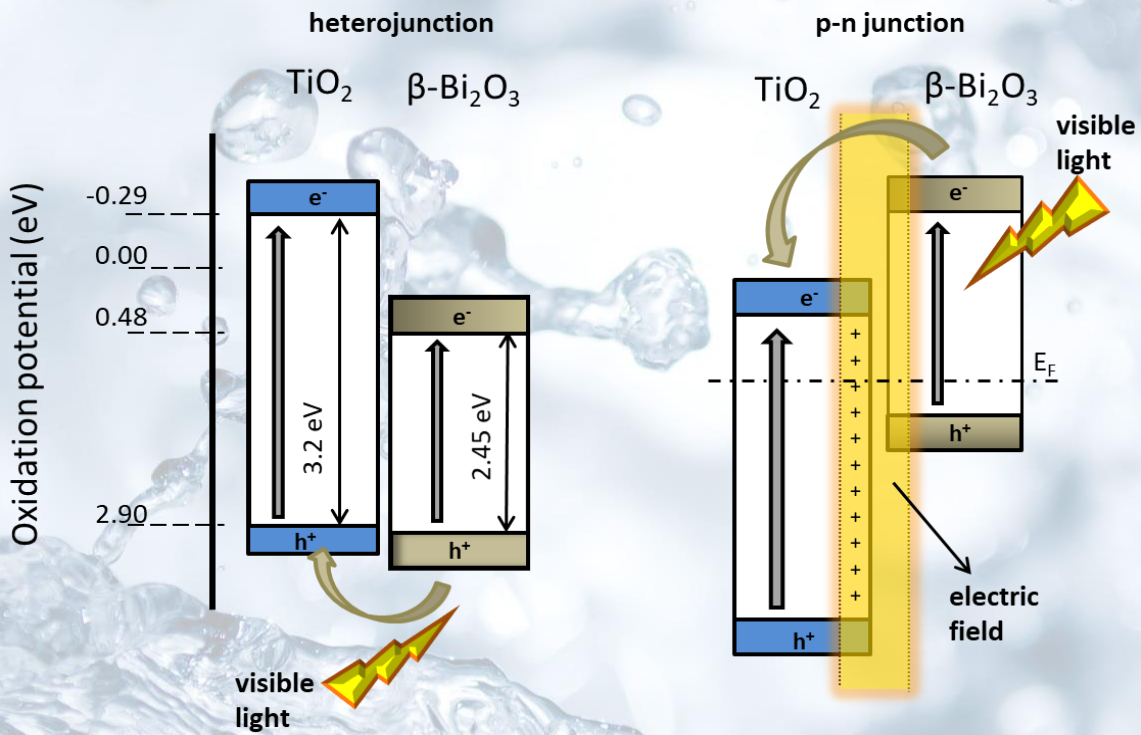

Fig. 15. Graphical illustration of a plausible charge carrier migration cascade at heterojunction in TiO_2-β-Bi_2O_3 composite and formation of the TiO_2/β-Bi_2O_3 p-n junction and the possible charge separation process under visible-light illumination.

Take home messages I

- **Solution combustion synthesis** was used to form a **junction** between **TiO_2** and **β-Bi_2O_3**
- β-Bi_2O_3 acts as **a visible-light photosensitizer** for TiO_2
- TiO_2 acts as a **scavenger** for β-Bi_2O_3 visible-light generated charge carriers
- **TiO_2-β-Bi_2O_3 junction** enables the transfer of photo generated charge carriers
- The composite significantly **enhances BPA oxidation** under **visible-light illumination**
- **Right amount** of β-Bi_2O_3 in the TiO_2-β-Bi_2O_3 composite is of crucial importance to achieve high catalytic activity

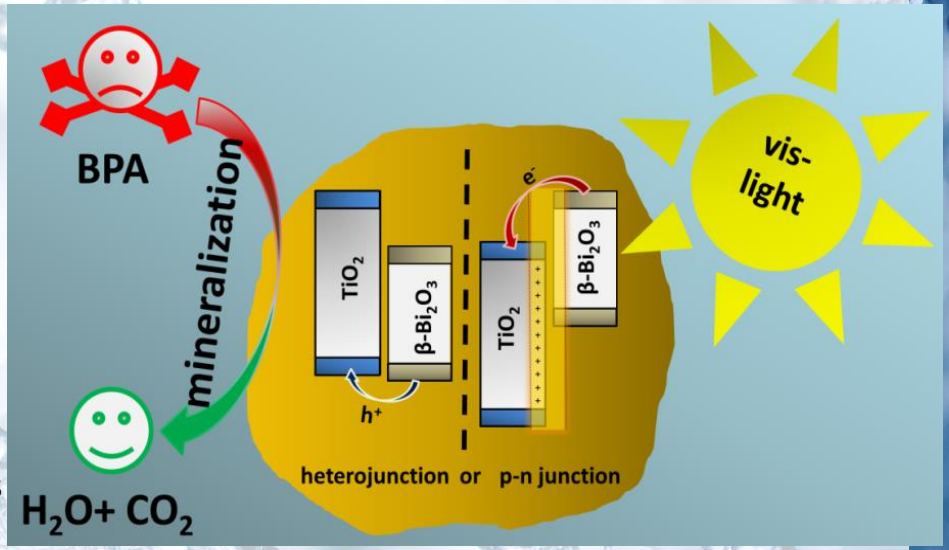

Žerjav et. A., *Catalysis today*, 2020, doi: 10.1016/j.cattod.2020.03.053.

different approaches to improve the catalytic activity of TiO_2 toward waste water treatment were tested:
combining with **reduced graphene oxide (rGO);** combining with **tungsten oxide (WO_3);**

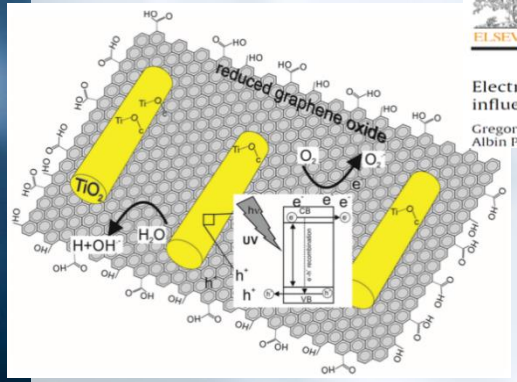

Applied Catalysis B: Environmental 209 (2017) 273–284
Contents lists available at ScienceDirect
Applied Catalysis B: Environmental
journal homepage: www.elsevier.com/locate/apcatb

Electron trapping energy states of TiO_2–WO_3 composites and their influence on photocatalytic degradation of bisphenol A

Gregor Žerjav[a,*], Muhammad Shahid Arshad[a], Petar Djinović[a], Janez Zavašnik[b], Albin Pintar[a]

Nanoscale
PAPER
View Article Online
View Journal | View Issue
Check for updates
Cite this: Nanoscale, 2017, 9, 4578

Improved electron–hole separation and migration in anatase TiO_2 nanorod/reduced graphene oxide composites and their influence on photocatalytic performance†

Gregor Žerjav,*[a] Muhammad Shahid Arshad,[a] Petar Djinović,[a] Ita Junkar,[b] Janez Kovač,[b] Janez Zavašnik[c] and Albin Pintar[a]

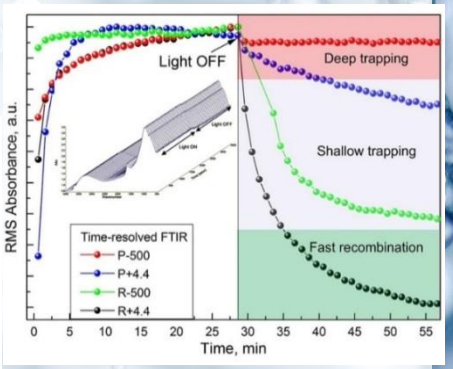

- decreased electron-hole recombination rate under UVA light illumination
- determination of the right amount of TiO_2 dopant is crucial to achieve efficient catalyst activity
- **the morphology of TiO_2 can influence the properties of a composite**

The main objective

- extend the use of **the solution combustion synthesis procedure** to the production of **TiO_2-Bi_2O_3** composites and to investigate how **TiO_2 supports with different morphologies and crystallinity influence the structural and electronic properties of prepared TiO_2-Bi_2O_3 composites** and how this impacts their **photocatalytic activity**.

Solution combustion synthesis procedure of the catalysts

dif. TiO_2 morphologies

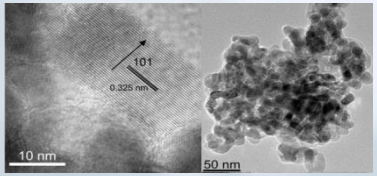

TNP*,#

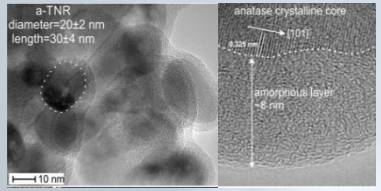

a-TNR#

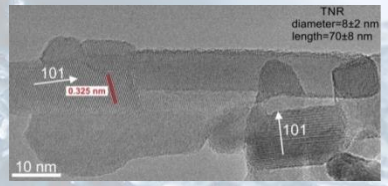

TNR#

*DT-51, Crystal company,
#Žerjav et al., Nanoscale 9 (2017) 4578-4592,
Žerjav et al., Appl. Catal. B 209 (2017) 273-284.

$Bi(NO_3)_3 * 5H_2O$
+
$C_6H_8O_7 * H_2O$
+
0.04 M HNO_3

↓ stirred for 1 h

PEG-5800

↓ stirred for 1 h

dif. TiO_2 morphologies

↓ stirred for 3 h

calcination 300 °C/4 h

ELSEVIER

Catalysis Today
Available online 9 April 2020
In Press, Corrected Proof

TiO_2-β-Bi_2O_3 junction as a leverage for the visible-light activity of TiO_2 based catalyst used for environmental applications

Gregor Žerjav [a], Janvit Teržan [a], Petar Djinović [a], Zuzana Barbieriková [b], Tomáš Hajdu [b], Vlasta Brezová [b], Janez Zavašnik [c, d], Janez Kovač [e], Albin Pintar [a]

↓

The optimal ratio between Ti and Bi was 1 : 0.4

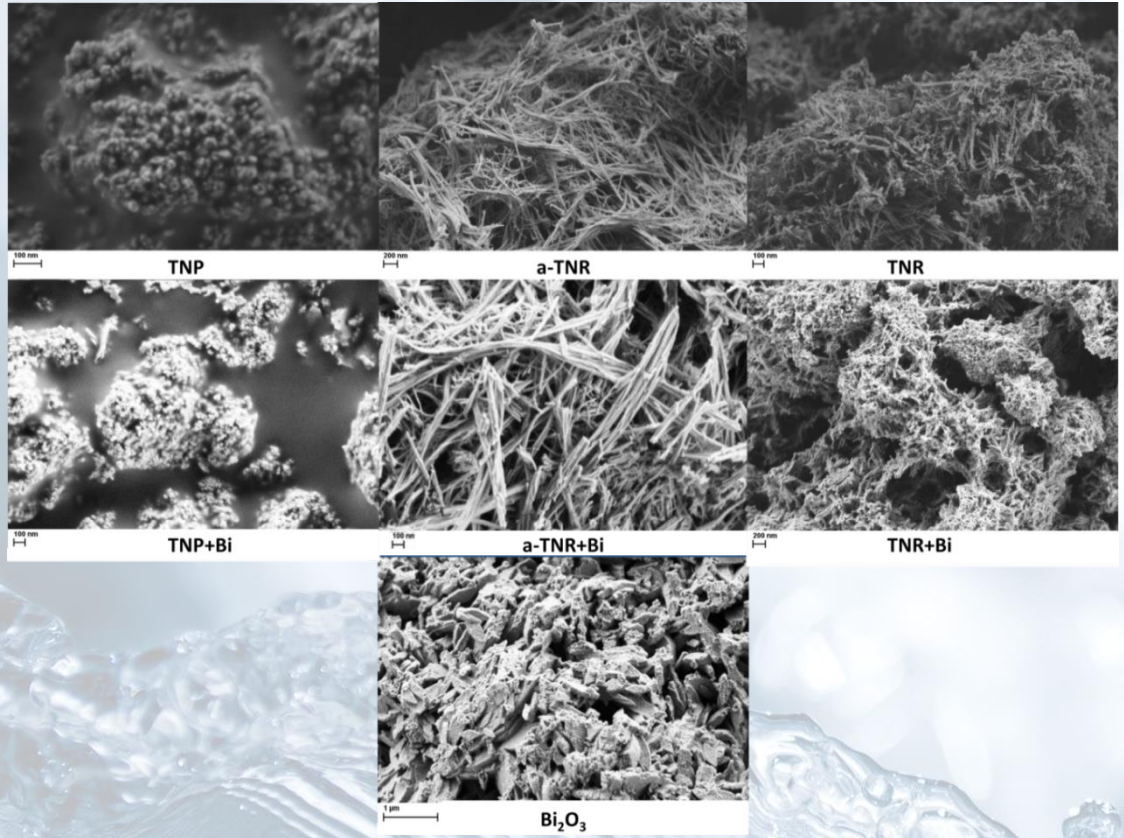

Fig. 16. SEM micrographs of prepared catalysts.

Sample	S_{BET} (m^2/g)	V_{pore} (cm^3/g)	d_{pore} (nm)
TNP	86	0.29	13.7
TNP+Bi	70	0.25	13.4
a-TNR	278	0.85	10.5
a-TNR+Bi	217	0.69	11.1
TNR	105	0.57	19.3
TNR+Bi	81	0.40	17.5
Bi_2O_3	4.7	0.02	16.5

Table 4. BET specific surface area (S_{BET}), total pore volume (V_{pore}) and average pore diameter (d_{pore}).

G. Žerjav, A. Pintar, 2020, MDPI Catalysts, 10, 395.

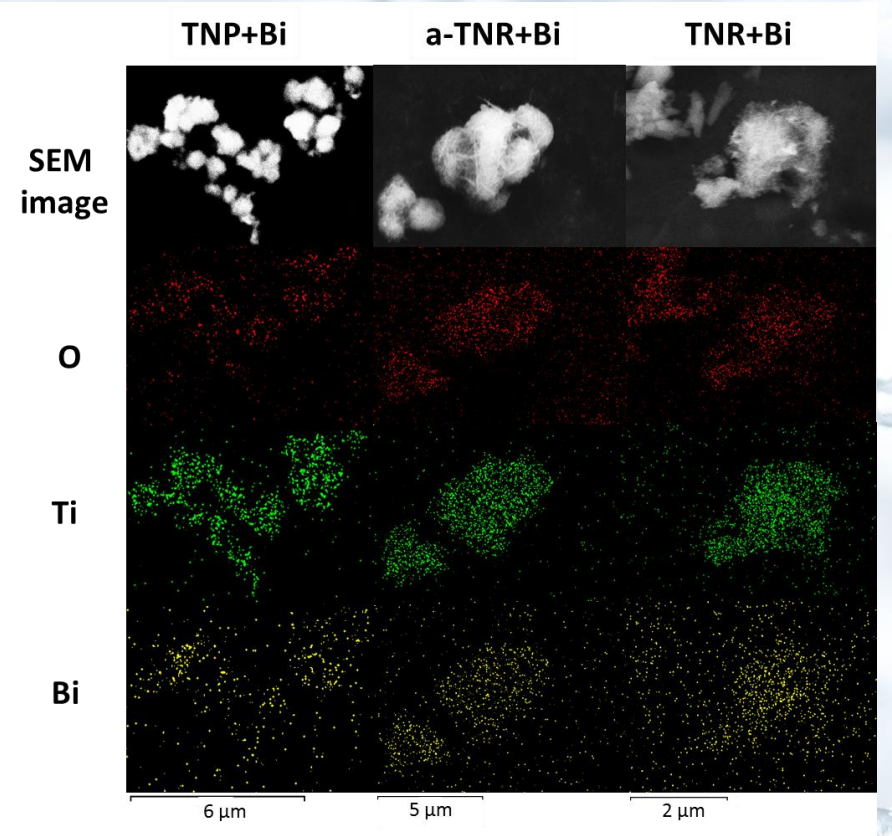

Fig. 17. SEM-EDX elemental mapping conducted on prepared TiO_2-Bi_2O_3 composites.

Sample	wt. %			Ti:Bi actual ratio
	O	Ti	Bi	
a-TNR+Bi	40	41	19	1:0.46
TNR+Bi	44	43	13	1:0.30
TNP+Bi	45	40	15	1:0.37

Table 5. Results of SEM-EDX analysis of the prepared catalysts.

G. Žerjav, A. Pintar, 2020, MDPI Catalysts, 10, 395.

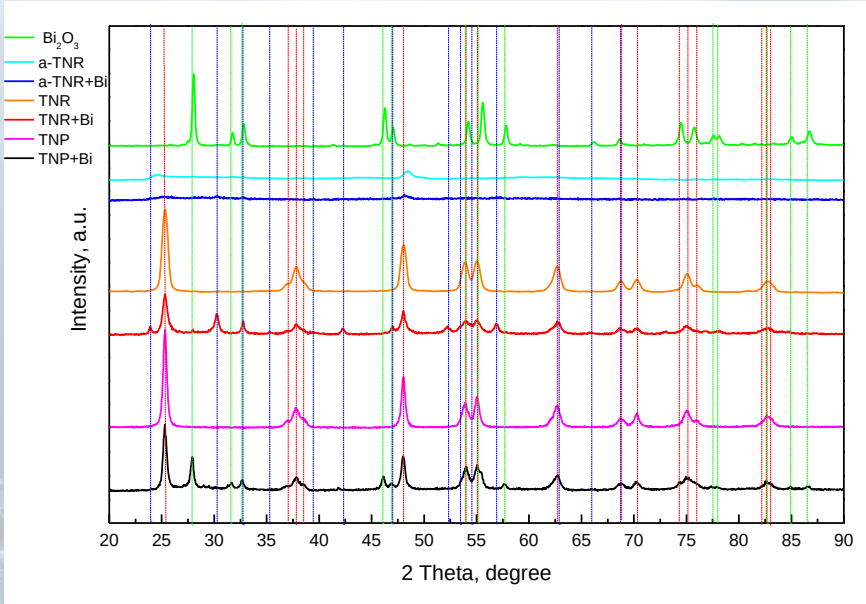

Fig. 18. XRD patterns of the prepared materials:
- green vertical lines belong to tetragonal β-Bi_2O_3,
- red vertical lines to anatase TiO_2 (JCPDS 00-021-1272),
- blue vertical lines to $(BiO)_2CO_3$ (JCPDS 00-025-1464).

Sample	Average crystallite size (nm)		
	[a] anatase TiO_2	[b] tetragonal β-Bi_2O_3	[c] $(BiO)_2CO_3$
TNP	20	/	/
TNP+Bi	20	25	/
a-TNR	/	/	/
a-TNR+Bi	/	[d] N.D.	N.D.
TNR	14	/	/
TNR+Bi	15	N.D.	18
Bi_2O_3	/	31	/

[a] Average crystallite size of anatase TiO_2 (JCPDS 00-021-1272).
[b] Average crystallite size of tetragonal β-Bi_2O_3 (JCPDS 00-027-0050).
[c] Average crystallite size of $(BiO)_2CO_3$ (JCPDS 00-041-1488).
[d] Not determined.

Table 6. Average crystallite size of anatase TiO_2, $(BiO)_2CO_3$ and tetragonal β-Bi_2O_3 in synthesized catalysts.

G. Žerjav, A. Pintar, 2020, MDPI Catalysts, 10, 395.

$$(BiO)_2CO_3 \rightarrow \beta\text{-}Bi_2O_3/(BiO)_2CO_3 \rightarrow \beta\text{-}Bi_2O_3 \rightarrow \beta\text{-}Bi_2O_3/\alpha\text{-}Bi_2O_3 \rightarrow \alpha\text{-}Bi_2O_3$$

3.1 eV 2.4 eV 2.8 eV

250 °C 300 °C 500 °C

Fig. 19. Temperature decomposition of $(BiO)_2CO_3$.*

*Zhu et al., 2015, New J. Chem., 39, 9557–9568.

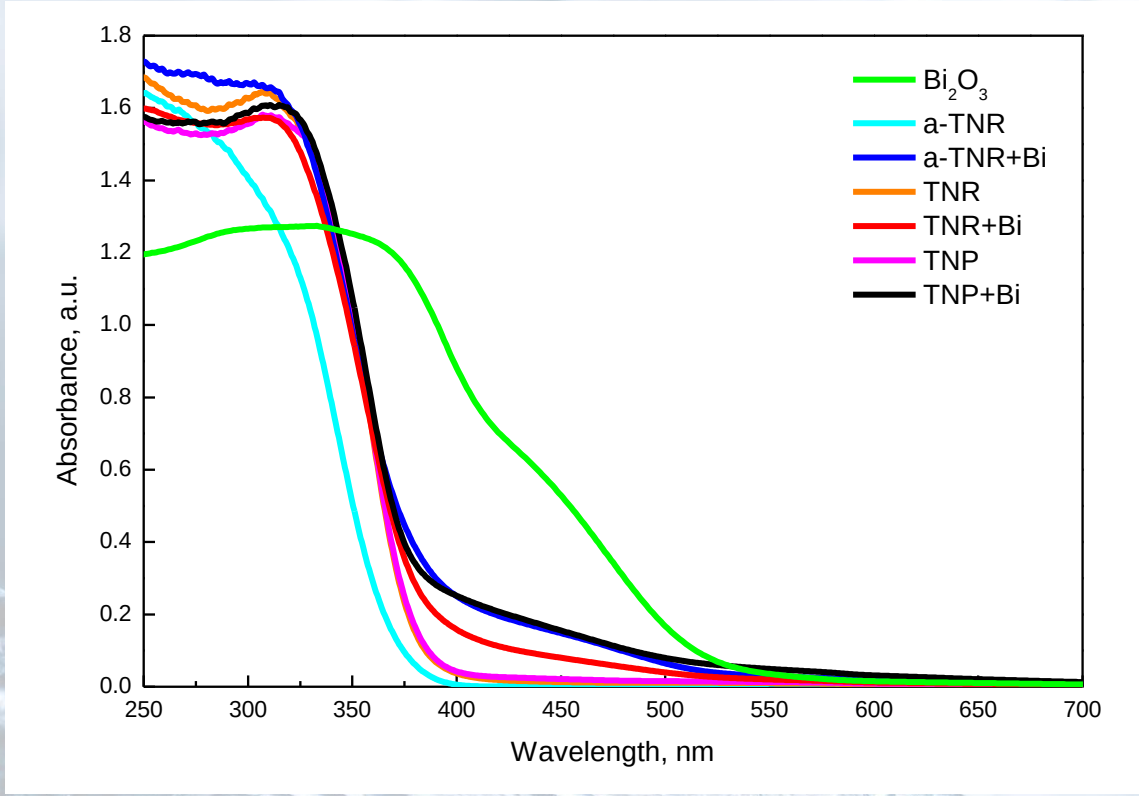

Fig. 20. UV-Vis DR spectra of synthesized catalysts.

Sample	Band gap (eV)
a-TNR	3.4
TNP	3.24
TNR	3.28
Bi_2O_3	2.45
$(BiO)_2CO_3$	3.1 -3.2[#]

[#] G. Zhu et. al, 2015, New J. Chem., 39, 9557-9568.

Table 7. Band gap energies of pure TiO_2 morphologies, β-Bi_2O_3 and $(BiO)_2CO_3$.

G. Žerjav, A. Pintar, 2020, MDPI Catalysts, 10, 395.

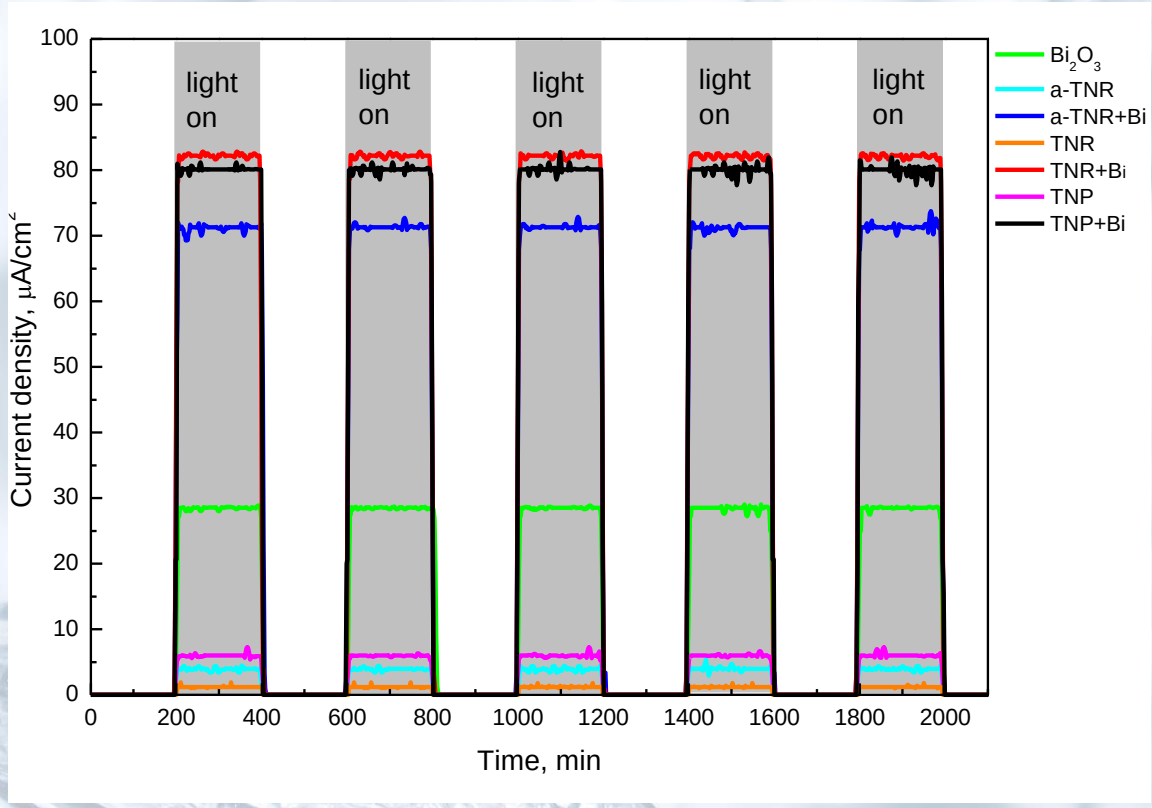

Fig. 21. Photocurrent densities at photoelectrode measured under intermittent visible light (LED light, grey area) irradiation in KOH (0.1 M).

G. Žerjav, A. Pintar, 2020, MDPI Catalysts, 10, 395.

Bisphenol A (BPA) degradation in a slurry batch reactor

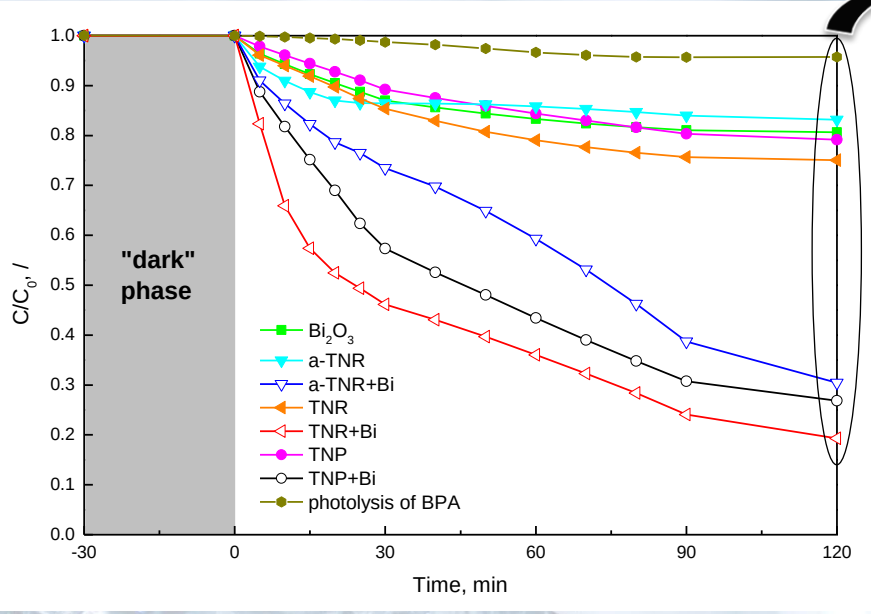

Fig. 22. Photocatalytic degradation of bisphenol A in the presence of prepared catalysts irradiated with visible light.

mineralization

Sample	TC_{spent}-TC_{fresh}	TOC_R (%)	TOC_M	TOC_A
TNP	0.04	/	/	/
TNP+Bi	0.16	23.0	20.0	3.0
a-TNR	0.74	/	/	/
a-TNR+Bi	0.3	21.0	16.0	5.0
TNR	0.45	11.0	4.0	7.0
TNR+Bi	0.51	51.0	43.0	8.0
Bi_2O_3	0.26	4.0	1.4	2.6

Table 8. Carbon content accumulated on the surface of composite catalysts before and after photocatalytic BPA degradation (TC_{spent}-TC_{fresh}). TOC removal (TOC_R) represents a sum of true TOC conversion (TOC_M) and TOC accumulation (TOC_A).

G. Žerjav, A. Pintar, 2020, MDPI Catalysts, 10, 395.

TNP+Bi

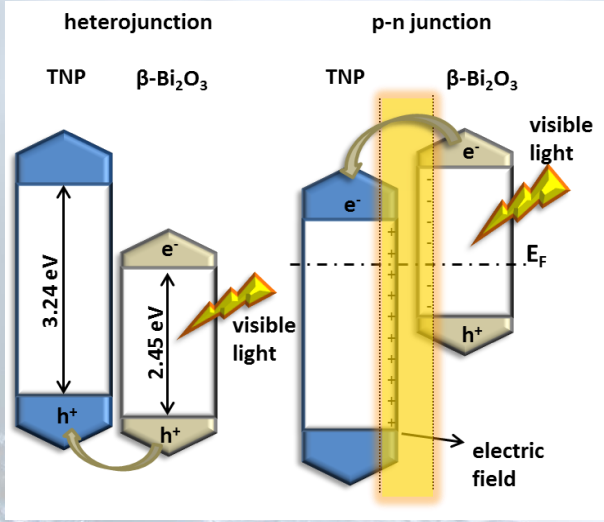

Fig. 23. Graphical illustration of a plausible charge carrier migration cascade at heterojunction in TiO_2-β-Bi_2O_3 composite and formation of the TiO_2/β-Bi_2O_3 and $(BiO)_2CO_3$/β-Bi_2O_3 p-n junction and the possible charge separation process under visible-light illumination.

G. Žerjav, A. Pintar, 2020, MDPI Catalysts, 10, 395.

TNP+Bi

TNR+Bi/a-TNR+Bi

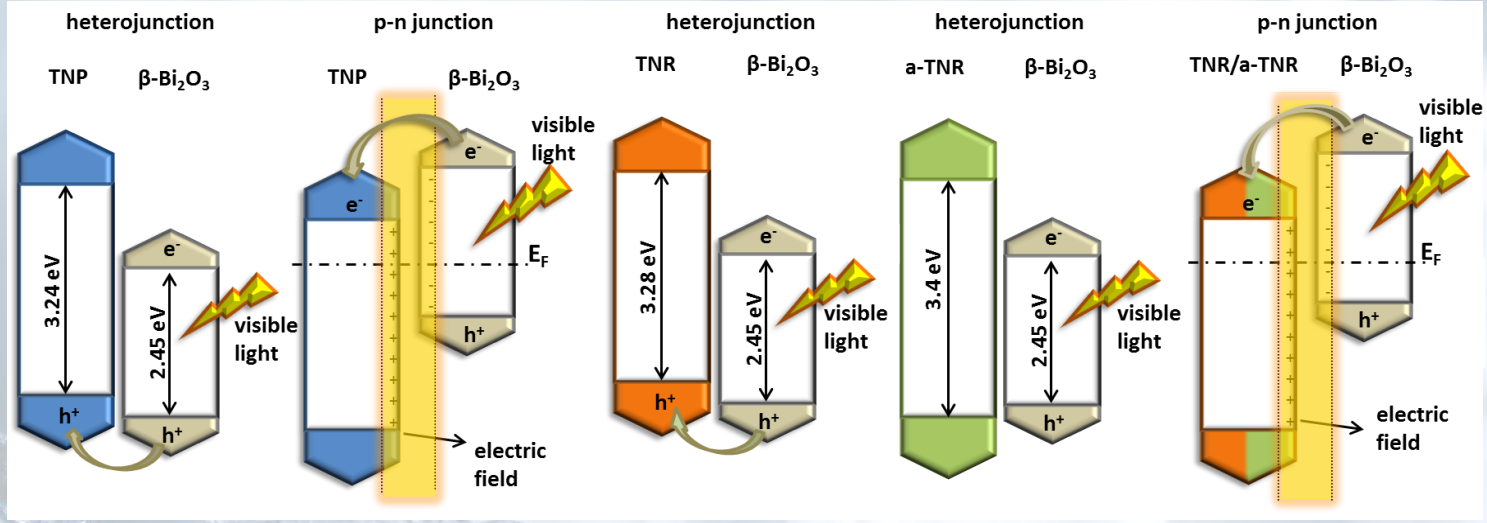

Fig. 23. Graphical illustration of a plausible charge carrier migration cascade at heterojunction in TiO_2-β-Bi_2O_3 composite and formation of the TiO_2/β-Bi_2O_3 and $(BiO)_2CO_3$/β-Bi_2O_3 p-n junction and the possible charge separation process under visible-light illumination.

G. Žerjav, A. Pintar, 2020, MDPI Catalysts, 10, 395.

TNP+Bi

TNR+Bi/a-TNR+Bi

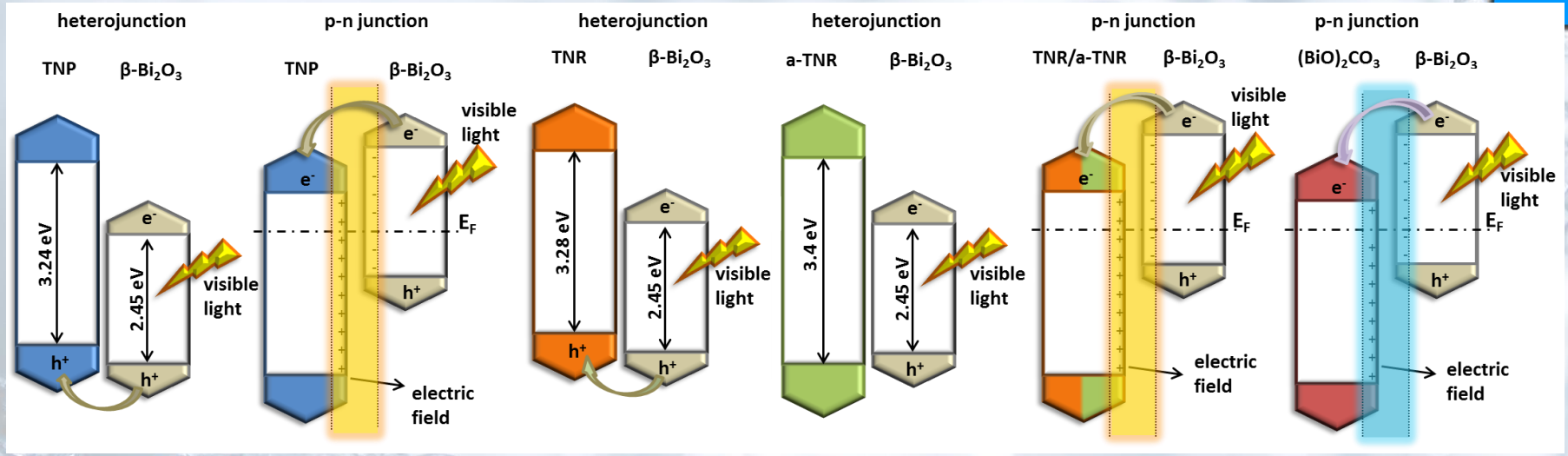

Fig. 23. Graphical illustration of a plausible charge carrier migration cascade at heterojunction in TiO_2-β-Bi_2O_3 composite and formation of the TiO_2/β-Bi_2O_3 and $(BiO)_2CO_3$/β-Bi_2O_3 p-n junction and the possible charge separation process under visible-light illumination.

G. Žerjav, A. Pintar, 2020, MDPI Catalysts, 10, 395.

Take home messages II

- when TNR and a-TNR are used is the supplied heat energy not sufficient to completely transform **$(BiO)_2CO_3$** into **β-Bi_2O_3**
- **solution combustion synthesis** was used to form a **junction** between **TiO_2 , $(BiO)_2CO_3$** and **β-Bi_2O_3**
- β-Bi_2O_3 acts as **a visible-light photosensitizer** for TiO_2 and $(BiO)_2CO_3$
- TiO_2 and $(BiO)_2CO_3$ acts as a **scavenger** for β-Bi_2O_3 visible light generated charge carriers;
- **TiO_2-β-Bi_2O_3-$(BiO)_2CO_3$ junction** enables the transfer of photo generated charge carriers;
- the composite significantly **enhances BPA oxidation** under **visible light illumination;**
- in the overall kinetics of photocatalytic BPA degradation is the hindered charge carrier recombination originating from the **crystallinity of TiO_2** more important factor than the **high specific surface area of the amorphous TiO_2** and **reduction/oxidation** of **surface adsorbed substrates**

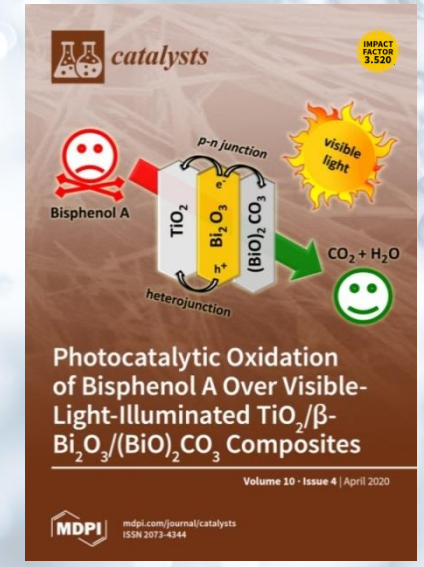

G. Žerjav, A. Pintar, 2020, MDPI Catalysts, 10, 395.

Formation of a junction between TiO_2 and β-Bi_2O_3 to enable efficient visible-light harvesting in advanced oxidation processes for waste water treatment

Gregor Žerjav

Department of Inorganic Chemistry and Technology,
National Institute of Chemistry, Ljubljana, Slovenia
gregor.zerjav@ki.si

NOWELTIES – 3rd Project Meeting & ATC2, 16th-18th September 2020, Zagreb, Croatia